Preferential oxidation of CO on a La-Co-Ru perovskite-type oxide catalyst

Rosa Pereñíguez,[1,2] Alfonso Caballero,[1] and Davide Ferri[2,3]

[1] Instituto de Ciencia de Materiales de Sevilla (CSIC-Universidad de Sevilla) and Dpto. Química Inorgánica (Universidad de Sevilla), Av. Américo Vespucio, 49, E-41092 Sevilla, Spain

[2] Swiss Federal Laboratories for Materials Science and Technology, Empa, Ueberlandstrasse 129, CH-8600 Dübendorf, Switzerland

[3] Paul Scherrer Institut, CH-5232 Villigen PSI, Switzerland

Abstract

A Ru-containing perovskite-type oxide La(Co,Ru)O_3 of nominal composition $LaCo_{0.8}Ru_{0.2}O_3$ was prepared by ultrasonic spray combustion and tested for the preferential oxidation of CO (PROX). EXAFS indicated that Ru adopted the coordination environment of Co in $LaCoO_3$ while Co was present as $LaCoO_3$ and Co_3O_4. PROX activity was replaced by CO hydrogenation activity above 250 ºC. Short oxidation at 500 ºC between temperature programmed reaction ramps did not restore the initial La(Co,Ru)O_3 structure but generated a catalyst with improved PROX activity compared to the initial La(Co,Ru)O_3. Under reductive PROX conditions the material experienced structural changes that improved its overall catalytic activity only if the catalyst was oxidized after each temperature programmed ramp.

Keywords: Ru; $LaCoO_3$; PROX; CO methanation; reduction; structural regeneration

Introduction

Perovskite-type oxides (ABO_3) are acknowledged as efficient catalysts for oxidation reactions [1-5]. It was recognized early that when doped with transition and precious metals this class of mixed oxides exerts a stabilizing function towards the dopant to avoid formation of volatile oxides and catalyst degradation. To this end, ruthenium was the major focus of studies already in the early 70's as it became a potential candidate for the removal of NO_x from treatment of exhaust gases of vehicles [6-8]. Moreover, the possibility to produce perovskite-type oxides with catalytically relevant B-site doping elements was shown to protect the metals from particle growth in automotive catalysis as a consequence of reversible segregation-incorporation within the perovskite-type structure [9]. Recently, the interest for Ru-doped perovskite-type oxides has been placed rather on high temperature applications such as fuel reforming [10-18] because of the thermal stability of perovskite-type oxides and the intrinsic activity of ruthenium. Fierro and co-workers [11-15] have shown that addition of Ru to $LaCoO_3$ improves especially the stability of the catalyst to high temperature reaction conditions. Because of the reducing environment of these reactions, the reducible $LaCoO_3$ can be used as an ideal catalyst precursor. During reaction or pretreatment, La_2O_3 or $La_2O_2CO_3$ supported Co and Ru particles are generated and constitute the final catalyst. The improved catalytic activity of Ru was attributed to the enhanced reducibility of $LaCoO_3$ by Ru and to the consequent improved formation of Co, Ru and possible Co-Ru metallic phases. This strategy could be exploited to generate suitable materials for catalytic processes operating at low and moderate temperatures. Therefore, in this work we use Ru-doped $LaCoO_3$ prepared by ultrasonic spray combustion [19, 20] as a possible catalyst for preferential oxidation of CO in excess hydrogen (PROX) in a broad temperature range. Ru is an active metal for this reaction [21] but it also catalyzes CO hydrogenation to CH_4 occurring at higher temperature than PROX [22]. Besides exploiting the reducibility of $LaCoO_3$

enabling the segregation of Ru, we show preliminary data on the structural regeneration of the catalyst, under sequential temperature programmed reaction and oxidation steps.

Experimental

An aqueous solution of $La(NO_3)_3 \cdot 6H_2O$ (Fluka, >99%), $Co(NO_3)_2 \cdot 6H_2O$ (Sigma–Aldrich, >98%), $RuCl_3 \cdot xH_2O$ (Aldrich >99%) and citric acid (Riedel-de Haën, >99.5%) in the necessary molar ratio to obtain $LaCoO_{3-\delta}$ and $LaCo_{0.8}Ru_{0.2}O_{3-\delta}$ ($La(Co,Ru)O_3$) was atomized in a ultrasonic nebulizer and transported by air flow through a vertical quartz reactor heated to 600 ºC [23]. The ratio between the amount of citric acid and the total amount of metal ions was 1. The resulting oxide powders were collected on a heated membrane filter (150 ºC) and calcined at 600 ºC for 4 h.

X-ray diffractograms (XRD) were recorded with a Philips X'pert Pro MPD diffractometer using Ni-filtered Cu Kα radiation (λ= 1.5418 Å). In situ XRD data during temperature programmed reduction (H_2-TPR) were collected at steady state in 5 vol% H_2/Ar up to 700 ºC (10 ºC/min) and 70 vol% H_2/N_2 up to 500°C (5 ºC/min) at temperature increments of 25 ºC (2θ range, 24–56º; step size, 0.05º). The BET specific surface area was measured from N_2 adsorption–desorption isotherms at -196 ºC using a Micromeritics ASAP 2020 instrument. Temperature programmed reduction (H_2-TPR) was performed in a setup equipped with a thermal conductivity detector (TCD) to quantify the H_2 concentration and an online mass spectrometer (MS) to monitor products formation [24]. CuO was used for quantification of the H_2 consumption. After heating in 5 vol% H_2/Ar to 700 ºC (10 ºC/min), cooling to room temperature and purging with He, the sample was heated in 3 vol% O_2/He to 700 ºC (10 ºC/min). This procedure was repeated three times and the reduction profiles were labelled as TPR-1, TPR-2 and TPR-3. Transmission extended X-ray absorption fine structure (EXAFS)

spectra were collected at the Co (7709 eV) and Ru (22117 eV) K-edges (BM01B beamline, ESRF, Grenoble) using Co and Ru foils for energy calibration.

The preferential oxidation of CO (PROX) was carried out by heating the catalyst (50 mg) in a quartz tubular reactor to 500 ºC (1 ºC/min) in 1 vol% O_2, 1 vol% CO and 70 vol% H_2, 100 mL/min (He balance). After cooling to room temperature, the catalyst was heated to 500 ºC in 20 vol% O_2/He followed by 5 min dwell at 500 ºC and cooling to room temperature. Five activity-oxidation cycles were performed that were followed by five activity cycles without intermediate oxidation (**Figure S1)**. The effluent gas was analyzed by gas chromatography (Varian GC-3800; TCD; Molecular Sieve 5 Å and Porapak®-N columns). CO and O_2 conversion, CO_2 yield and CH_4 yield were determined as follows:

$$X(CO)\ (\%) = 100 \times (nCO_{in} - nCO_{out})/nCO_{in}$$

$$X(O_2)\ (\%) = 100 \times (nO_{2in} - nO_{2out})/nO_{2in}$$

$$Y(CO_2)\ (\%) = 100 \times nCO_{2out}/nCO_{in}$$

$$Y(CH_4)\ (\%) = 100 \times nCH_{4out}/nCO_{in}$$

where *n*i is the amount of every component (i) in moles.

Results and Discussion

The XRD pattern of $La(Co,Ru)O_3$ (30.2 m^2/g) calcined at 600 ºC exhibited only the reflections of the rhombohedral structure of $LaCoO_3$ (ICDD, 01-084-0847, R-3c; **Figure 1**). The missing doublets characteristic of the rhombohedral structure reflected the low degree of criystallinity as a result of the low synthesis and calcination temperatures. The significant shift to lower 2θ values of the reflections compared to $LaCoO_3$ suggests that Ru was inserted at the B-site [12]. The edge energy (7723 eV) of the Co K-edge XANES spectrum of

$La(Co,Ru)O_3$ (**Figure 2)** was intermediate between that of $LaCoO_3$ (Co^{3+}, 7724 eV) and Co_3O_4 ($Co^{2+/3+}$, 7717 eV). The whiteline presented a second peak attributable to Co_3O_4. Beside the Co-O coordination shell at 1.5 Å, which did not match that of Co_3O_4 (1.7 Å), the peak at ca. 3.2 Å that is due to multiple contributions of Co-La, Co-Co, and Co-O-Co bonds was weaker than in $LaCoO_3$ in the FT-EXAFS spectrum (**Figure 2**) suggesting a large degree of disorder induced by Co substitution [25]. The contribution at 2.5 Å resembled the coordination environment of cobalt in Co_3O_4. These observations suggest the presence of a mixed local environment of Co and the coexistence of $LaCoO_3$ and Co_3O_4 phases in $La(Co,Ru)O_3$. Its dispersion and amorphous character, reflecting the structural disorder observed in the FT-EXAFS of $La(Co,Ru)O_3$ explain the absence of Co_3O_4 in the XRD (**Figure 1**).

The Ru K-edge XANES spectrum of $La(Co,Ru)O_3$ (**Figure 2**) did not match the spectra of reference materials with nominal Ru oxidation state +3 ($RuCl_3$) and +4 (RuO_2). It was composed of two major peaks due to $1s \rightarrow 5p_x$ and $1s \rightarrow 5p_{y(z)}$ transitions in distorted RuO_6 octahedra in perovskites [26], implying that Ru adopted the oxidation and coordination states of the B-site. By comparison of the position of the maximum of the first derivative of $La(Co,Ru)O_3$ with that of compounds with oxidation state +3 ($RuCl_3$), +4 (RuO_2), +4.5 ($Pb_2Ru_2O_{6.5}$) and +5 (Ca_2YRuO_6) (**Figure 2**)[27], we assign Ru an oxidation state close to +5 and octahedral coordination. This oxidation state could be justified by the similar ionic radius of Ru^{5+} (0.705 Å) in octahedral coordination and Co^{3+} (0.685 Å) compared to lower oxidation states of Ru (Ru^{4+}: 0.76 Å or Ru^{3+}: 0.82 Å) [28]. The slightly larger radius of Ru^{5+} induces the shift to lower diffraction angles in the XRD. Because no Ru K-edge spectrum was reported, we could not compare our spectra with those measured by Mota et al. [13], who proposed Ru^{+4} in $LaCo_{0.8}Ru_{0.2}O_3$. The high oxidation state of Ru is consistent with the large degree of disorder evident from the FT spectrum of the Co K-edge and the partial reduction

of Co^{3+} to Co^{2+} related to the presence of Co_3O_4. Charge compensation/redistribution and the unit cell distortion can suggest the Co segregation if all Ru adopted the coordination state of Co and was all integrated in the perovskite lattice. Assuming that Co was present only in oxidation state +3 in the perovskite phase, while Ru was in the oxidation state +5 and all exchanged in the perovskite phase, the stoichiometry of the B-site should be $Co^{3+}_{0.67}Ru^{5+}_{0.2}$ (overall oxidation state of B-site, +3) rather than the theoretical $Co^{3+}_{0.8}Ru^{5+}_{0.2}$ (+3.4). The difference of Co concentration in the perovskite is thus compensated by the formation of Co_3O_4.

The H_2-TPR profile of $La(Co,Ru)O_3$ exhibited three major peaks (TPR-1, **Figure 3**) and Ru improved the reducibility of $LaCoO_3$ in agreement with previous observations [12]. According to the H_2 consumption values and after deconvolution of the different contributions of TPR-1 (**Table S1**), we assume that the reduction of the cobalt phase took place in two steps, i.e. $Co^{2.95+} \rightarrow Co^{2+}$ (375 ºC) and $Co^{2+} \rightarrow Co^0$ (>500 ºC). The first peak at 295 ºC is ascribed to the reduction of ruthenium. The values of theoretical ($\Delta n_T^+ = 1$) and experimental ($\Delta n_E^+ = 0.81$) extent of electron exchange for this step suggest that reduction of ruthenium may have been partial and could have been completed together with the subsequent step, the reduction of cobalt (375 ºC). For the peak at 375 ºC we measured an excess of H_2 consumption ($\Delta n_E^+ = 1.13$ against $\Delta n_T^+ = 0.76$). Segregated Ru^0 promoted likely the first reduction peak of cobalt (250-450 ºC) by hydrogen spillover. The second (TPR-2) and third (TPR-3) H_2-TPR profiles were different compared to TPR-1. The two H_2 consumption peaks below 400 ºC of TPR-1 merged in a sharp peak centered at ca. 350 ºC. Similarly, the clear event at 550 ºC became a shoulder of the peak at 605 ºC, which shifted to ca. 590 ºC. It is evident that TPR-2 and TPR-3 are very similar suggesting the structural reversibility of the material over redox cycles after the first reduction segment. Therefore, the

short oxidation at 700 ºC did not restore completely the initial structure obtained after synthesis and calcination at 600 ºC.

In order to explain these differences, in situ XRD was carried out during H_2-TPR in 5 vol% H_2 (**Figure 4**). Ideally the structural changes should coincide with the reduction events observed in **Figure 3**. At ca. 400 ºC the rhombohedral $LaCoO_3$ structure vanished in favor of the oxygen deficient $La_2Co_2O_5$. La_2O_3 appeared already at 500 ºC; at 700 ºC there was no remaining reflection of a perovskite-type oxide. However, no Ru-phase and Co^0 were detected indicating that Ru and Co were well dispersed on La_2O_3. Therefore, the results confirm that the first H_2-TPR peak corresponds to the reduction of Ru^{5+} and of Co^{3+} ($Ru/LaCoO_3$) to Co^{2+} ($Ru/La_2Co_2O_5$), while the peak at higher temperature belongs to the complete reduction of cobalt and loss of the perovskite phase. **Figure S2a** and **Figure S2b** show the diffractograms of calcined $La(Co,Ru)O_3$ and of the sample after one in situ XRD redox cycle, respectively. The diminished intensity of the reflections indicated that the short oxidation at 700 ºC and the subsequent cooling in the same environment generated a more disordered perovskite structure. However, without any other experimental evidence, we speculate that the same 2θ position of the diffraction peaks suggests that Ru reverted in the perovskite structure.

$La(Co,Ru)O_3$ was subjected to a sequence of consecutive temperature programmed ramps in the preferential CO oxidation (PROX) feed alternated to temperature programmed oxidation ramps (**Figure S1**). Under similar reducing conditions of PROX, an in situ XRD measurement with 70 vol% H_2 (**Figure S3**) demonstrated the same phase transitions observed with 5 vol% H_2 but at lower temperature: $La_2Co_2O_5$ was observed at 200 ºC and reduction to La_2O_3 occurred at ca. 500 ºC.

Figure 5 shows the CO conversion data for the preferential CO oxidation (PROX), while **Figure S4** displays the O_2 conversion and CO_2 yield data. In the first PROX profile (R1) the

reaction was initiated above 200 ºC and 90% CO conversion was attained at 350 ºC. The relatively broad temperature window in which activity was measured allowed capturing a change of reaction regime from the preferential CO oxidation to CO methanation above 300 ºC [29]. The activity profiles obtained after the first oxidation including heating and cooling segments to 500 ºC (R2-R5) demonstrated that the temperature regime for PROX shifted to lower temperature by ca. 100 ºC (CO conversion, **Figure 5**; O_2 conversion, **Figure S4**). Full CO conversion was reached at 300 ºC just before activity loss. The kink in the CO conversion at 200 ºC corresponded to the maximum CO_2 yield. Comparison of **Figure 5** and **Figure S4** suggests that between 50 and 200°C PROX dominated over H_2 combustion though the stoichiometry of the reactions indicates that the latter was occurring parallel to PROX to some extent. CO methanation replaced CO oxidation above 250 ºC after the first activity run (**Figure S4**). The loss of activity above 350 ºC mirrored the decrease of CH_4 yield. The activity profiles remained substantially unchanged after R2 confirming that the structural changes did not proceed further. This observation is in agreement with the H_2-TPR data of **Figure 4** showing that consecutive TPR profiles after the first and reoxidation (700 ºC) were very similar.

In absence of further in situ characterization data, the observed activation can be explained as follows. The reduction of the perovskite-type structure during the temperature programmed reaction under reducing conditions (70 vol% H_2) to 500 ºC caused the reduction and segregation of Ru^0 and the formation of a Ru^0-Co^0/La_2O_3 catalyst. We cannot conclude whether a Ru-Co alloy was formed. After oxidation at 500 ºC, that is milder than the temperatures of synthesis and initial calcination, part of the material was restored into A- and B-site deficient $LaCoO_3$ and this was likely not sufficient to revert completely to the initial oxidation and coordination environment, however this treatment results in a better catalyst. The subsequent H_2-TPR experiments (**Figure 4**) then could correspond predominantly to

reduction of oxidized Ru and $LaCoO_3$ together with the incorporated Ru ($La(Co,Ru)O_3$) and Co_3O_4. In the case of the catalytic activity, the consecutive temperature programmed ramps after the first oxidation involved most likely $yRuO_2/La_yCo_{1-x}Ru_{x-y}O_3/(1-y)La_2O_3$ rather than $La(Co,Ru)O_3$ that reduced upon heating under reducing conditions generating Ru^0 particles. We cannot exclude that also a fraction of Co^0 obtained at the end of the reaction run at 500 ºC could have been oxidized to Co_3O_4 rather than $LaCoO_3$ and that therefore the activity is influenced by both Ru^0 and Co^0 species. The segregated metal phase is responsible for the CO hydrogenation activity above 250 ºC.

When no intermediate oxidation was carried out, catalytic activity declined (**Figure 5**). After the shift to lower temperature in R6, maximum CO conversion (70%) was measured at 290 ºC and was accompanied by an increase in reaction temperature. CH_4 was the major product. Without spectroscopic results on the sample after each activity run, we can only speculate that Ru^0-Co^0/La_2O_3 obtained under reducing conditions at the end of the activity run was subject to metal particle growth. The presence of reduced metals under these conditions is responsible for the selective CO hydrogenation.

We infer, from the characterization and activity data, that without pretreatment the structure of $La(Co,Ru)O_3$ changes during reaction due to the reducing conditions, generating an active material for CO hydrogenation. Hence, $La(Co,Ru)O_3$ can be used as catalyst precursor for PROX (oxidized catalyst) and CO methanation (reduced catalyst). Strategies are available to regenerate the initial material for example to avoid metal particle growth or even poisoning. Short mid temperature oxidation (500 ºC, after PROX) is able to regenerate only partly the initial structure, but this is sufficient to generate a more active catalyst for PROX. On the contrary, continuous reducing conditions are less favourable for the generation of an active catalyst for PROX and CO hydrogenation is promoted.

Acknowledgments

The authors kindly acknowledge the financial support from the Spanish Ministry of Research (Project CTQ2014-60524-R), the University of Seville for a scholarship for R.P. and the Swiss National Science Foundation (SNF). The European Synchrotron Research Facility (ESRF) is acknowledged for beamtime allocation at the Swiss-Norwegian beamline (SNBL). The assistance of Dr. A. Kambolis and A. Rodriguez-Gomez during beamtime is highly appreciated.

References

[1] G. Parravano, J. Am. Chem. Soc., 75 (1953) 1497.

[2] D.W. Johnson, P.K. Gallagher, Thermochimica Acta, 7 (1973) 303.

[3] R.J.H. Voorhoeve, J.P. Remeika, P.E. Freeland, B.T. Matthias, Science, 177 (1972) 353.

[4] S. Royer, D. Duprez, ChemCatChem, 3 (2011) 24.

[5] N. Yamazoe, Y. Teraoka, Catal. Today, 8 (1990) 175.

[6] M. Skoglundh, L. Lowendahl, K. Jansson, L. Dahl, M. Nygren, Appl. Catal. B:Environmental, 3 (1994) 259.

[7] L.E. Trimble, Mater. Res. Bull., 9 (1974) 1405.

[8] R.J.H. Voorhoeve, J.P. Remeika, L.E. Trimble, Mater. Res. Bull., 9 (1974) 1393.

[9] Y. Nishihata, J. Mizuki, T. Akao, H. Tanaka, M.-. Uenishi, M. Kimura, T. Okamoto, N. Hamada, Nature, 418 (2002) 164.

[10] D.J. Liu, M. Krumpelt, Int. J. Appl. Technol., 2 (2005) 301.

[11] N. Mota, M.C. Alvarez-Galvan, S.M. Al-Zahrani, R.M. Navarro, J.L.G. Fierro, Int. H. Hydr. En., 37 (2012) 7056.

[12] N. Mota, M.C. Alvarez-Galván, R.M. Navarro, S.M. Al-Zahrani, A. Goguet, H. Daly, W. Zhang, A. Trunschke, R. Schlögl, J.L.G. Fierro, Appl. Catal. B:Environmental, 113-114 (2012) 271-280.

[13] N. Mota, L. Barrio, C. Alvarez-Galvan, F. Fauth, R.M. Navarro, J.L.G. Fierro, J. Phys. Chem. C, 119 (2015) 16708-16723.

[14] N. Mota, R.M. Navarro, M.C. Alvarez-Galvan, S.M. Al-Zahrani, J.L.G. Fierro, J. Power Sources, 196 (2011) 9087-9095.

[15] R.M. Navarro, M.C. Alvarez-Galvan, J.A. Villoria, I.D. Gonzalez-Jimenez, F. Rosa, J.L.G. Fierro, Appl. Catal. B:Environmental, 73 (2007) 247.

[16] H.R. Gurav, R. Bobade, V.L. Das, S. Chilukuri, Ind. J. Chem., 51A (2012) 1339.

[17] E. Pietri, A. Barrios, O. Gonzalez, M.R. Goldwasser, M.J. Perez-Zurita, M.L. Cubeiro, J. Goldwasser, L. Leclercq, G. Leclercq, L. Gingembre, Stud. Surf. Sci. Catal., 136 (2001) 381.

[18] M.R. Goldwasser, M.E. Rivas, E. Pietri, M.J. Perez-Zurita, M.L. Cubeiro, L. Gingembre, L. Leclercq, G. Leclercq, Appl. Catal. A:General, 255 (2003) 45.

[19] R. Pereniguez, V.M. Gonzalez-delaCruz, A. Caballero, J.P. Holgado, Appl. Catal. B:Environmental, 123 (2012) 324-332.

[20] D. Ferri, A. Heel, D. Burnat, Aerosol spray synthesis of perovskite-type oxides, in Perovskites and related mixed oxides: concepts and applications, P. Granger, V.I. Parvulescu, S. Kaliaguine, W. Prellier (Eds.), Wiley-VCH Verlag GmbH & Co. KGaA, 2016, pp. 69.

[21] S.H. Oh, R.M. Sinkevitch, J. Catal., 142 (1993) 254.

[22] E.D. Park, D. Lee, H.C. Lee, Catal. Today, 139 (2009) 280.

[23] X. Wei, P. Hug, R. Figi, M. Trottmann, A. Weidenkaff, D. Ferri, Appl. Catal. B:Environmental, 94 (2010) 27-37.

[24] P. Malet, A. Caballero, J. Chem. Soc., Faraday Trans. I, 84 (1988) 2369-2375.

[25] J.L. Hueso, J.P. Holgado, R. Pereniguez, S. Mun, M. Salmeron, A. Caballero, J. Solid State Chem., 183 (2010) 27-32.

[26] M. Mizumaki, K. Yoshii, Y. Hinatsu, Y. Doi, T. Uruga, Phys. Scripta, T115 (2005) 513.

[27] T. Vitova, S. Mangold, C. Paulmann, M. Gospodinov, V. Marinova, B. Mihailova, Phys. Rev. B, 89 (2014).

[28] R.D. Shannon, Acta Crystallogr. Sect. A, 32 (1976) 751-767.

[29] X. Chen, J.J. Delgado, J.M. Garcia, S. Zerrad, J.M. Cies, S. Bernal, J. Catal., 299 (2013) 272-283.

Figure captions

Figure 1. X-ray diffraction patterns of $LaCoO_3$ and $La(Co,Ru)O_3$. The right panel details the major reflection line.

Figure 2. Co K-edge XANES, non-phase shift corrected FT-EXAFS spectra of $LaCoO_3$ and $La(Co,Ru)O_3$, Ru K-edge XANES spectra of $La(Co,Ru)O_3$ and reference compounds, and first derivative of the Ru K-edge XANES spectra of $La(Co,Ru)O_3$ and reference compounds.

Figure 3. Temperature-programmed reduction profiles of $La(Co,Ru)O_3$. The bottom profile belongs to $LaCoO_3$.

Figure 4. In situ XRD patterns of $La(Co,Ru)O_3$ recorded during H_2-TPR with 5 vol% H_2. Symbols: (▽) hexagonal La_2O_3; (○) distorted rhombohedral $LaCoO_3$, (✳) brownmillerite $La_2Co_2O_5$.

Figure 5. CO conversion in consecutive PROX activity measurements of $La(Co,Ru)O_3$ (a) with and (b) without intermediate oxidation at 500 ºC. Profiles marked with * are the ones shown in (a).

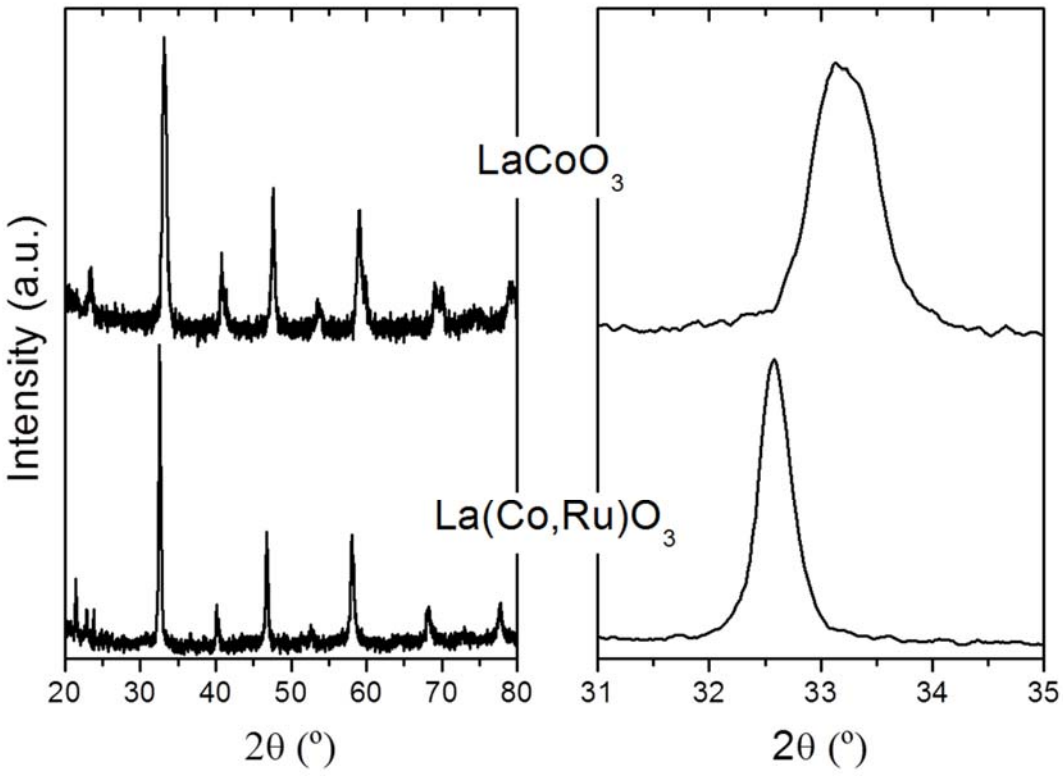
LaCoO3
La(Co,Ru)O3
Intensity (a.u.)
20
30
40
50
60
70
80
31
32
33
34
35
2θ (º)
2θ (º)

Figure 1

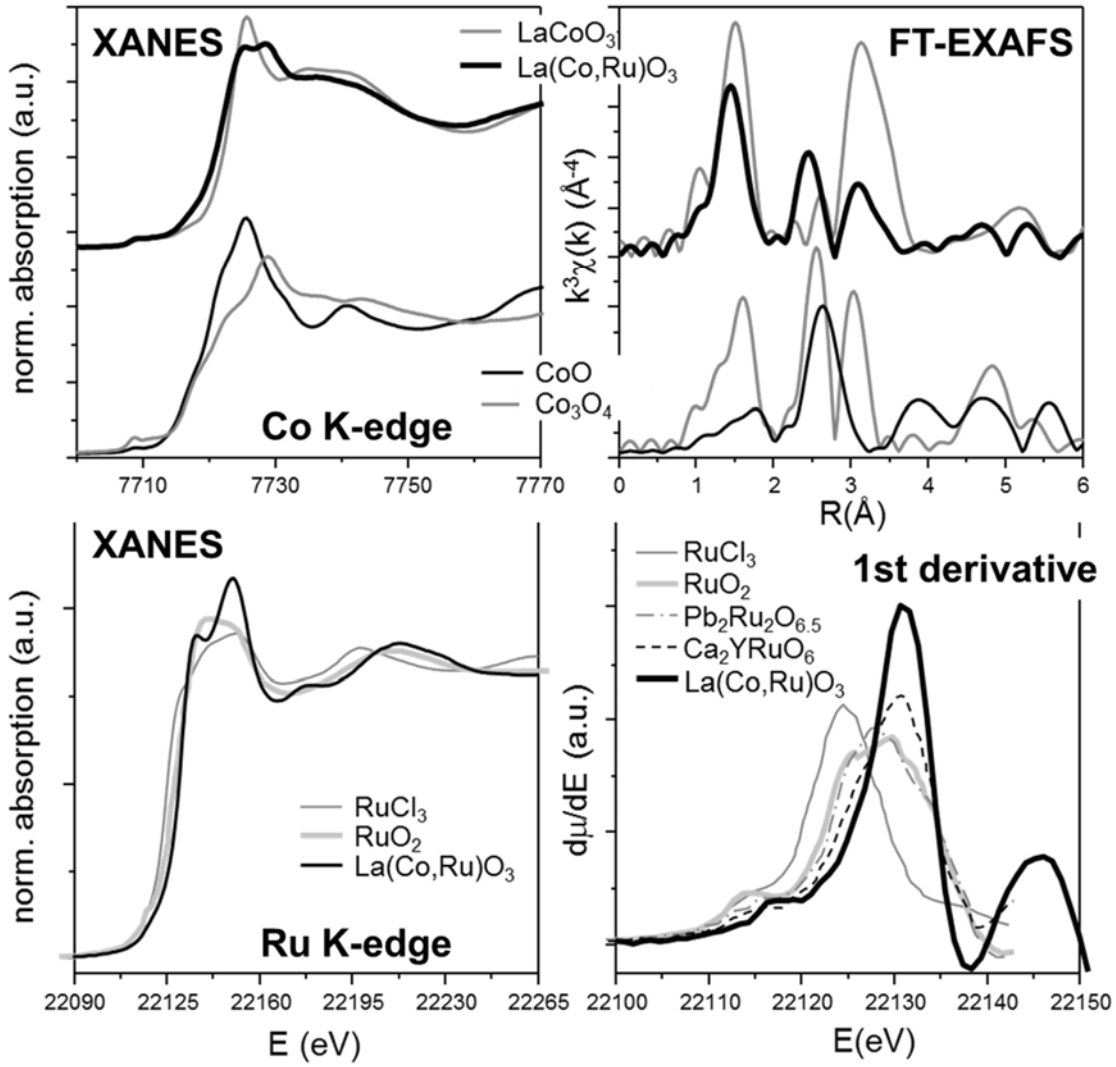
XANES
LaCoO3
La(Co,Ru)O3
CoO
Co3O4
Co K-edge
norm. absorption (a.u.)
7710
7730
7750
7770
FT-EXAFS
k3χ(k) (Å-4)
R(Å)
XANES
RuCl3
RuO2
La(Co,Ru)O3
Ru K-edge
norm. absorption (a.u.)
E (eV)
1st derivative
Pb2Ru2O6.5
Ca2YRuO6
dμ/dE (a.u.)
E(eV)

Figure 2

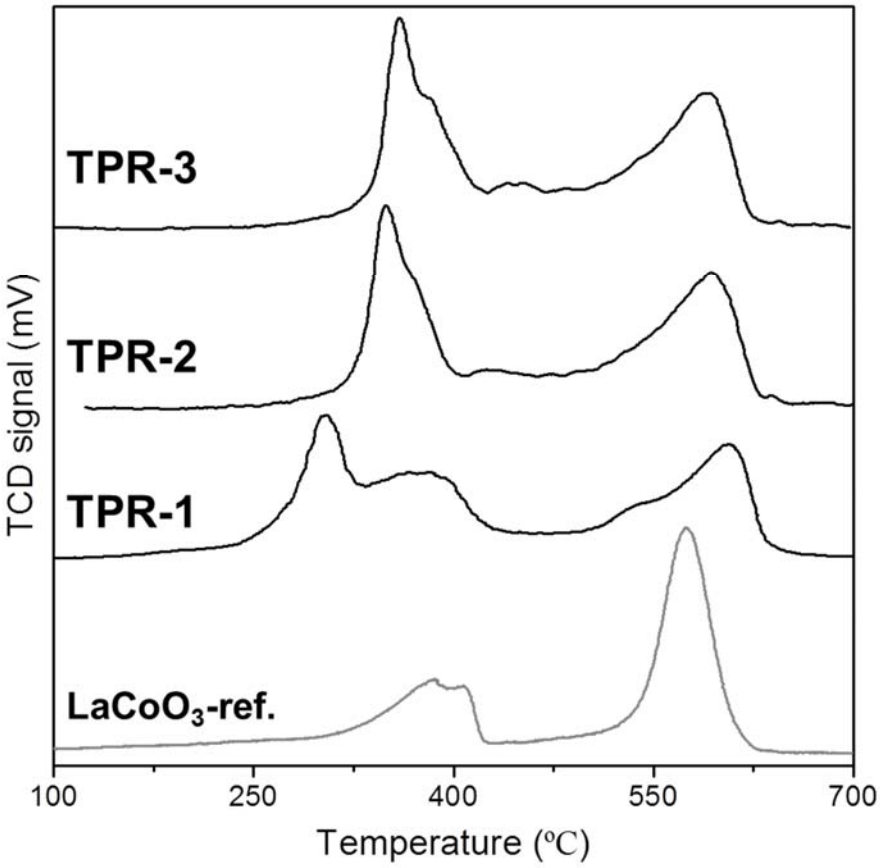
TPR-3
TPR-2
TPR-1
LaCoO3-ref.
TCD signal (mV)
100
250
400
550
700
Temperature (°C)

Figure 3

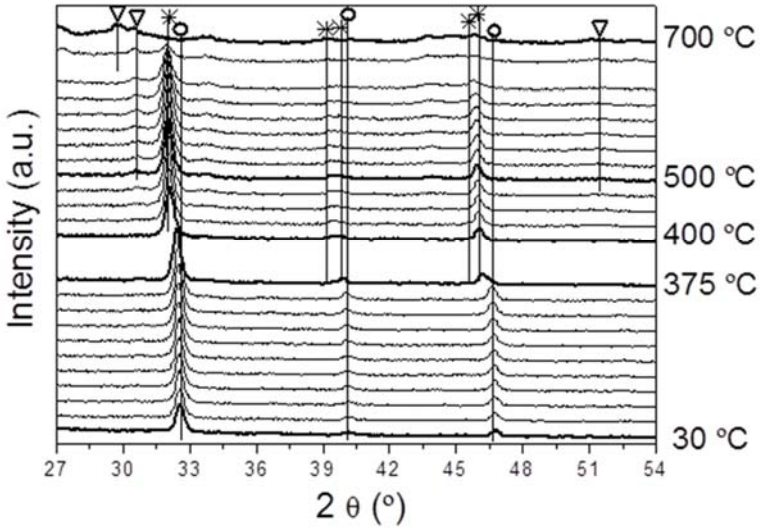
Intensity (a.u.)
700 °C
500 °C
400 °C
375 °C
30 °C
27
30
33
36
39
42
45
48
51
54
2 θ (°)

Figure 4

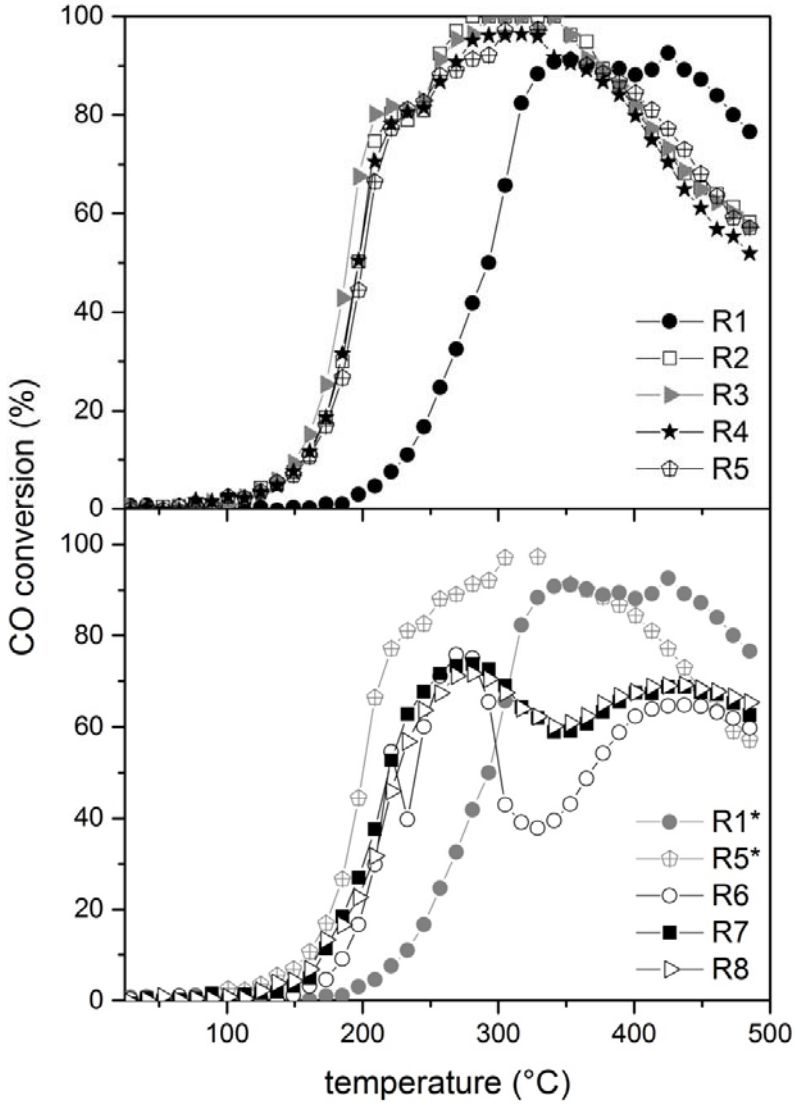

Figure 5